Carbohydrate Polymer Technologies and Applications 4 (2022) 100227

Contents lists available at ScienceDirect

Carbohydrate Polymer Technologies and Applications

journal homepage: www.sciencedirect.com/journal/carbohydrate-polymer-technologies-and-applications

Amino acid decorated xanthan gum coatings: Molecular arrangement and cell adhesion

Alex Carvalho Alavarse [a], Emilli Caroline G Frachini [a], Jean Bezerra Silva [b], Rafael dos Santos Pereira [c], Henning Ulrich [b], Denise Freitas Siqueira Petri [a,*]

[a] Fundamental Chemistry Department, Institute of Chemistry, University of São Paulo, Av. Prof. Lineu Prestes 748, São Paulo, 05508-000, Brazil
[b] Department of Biochemistry, Institute of Chemistry, University of São Paulo, Av. Prof. Lineu Prestes 748, São Paulo,05508-000, Brazil
[c] Nanosciences and Advanced Materials, Federal University of ABC, Av. Dos Estados 5001, Santo André, 09210-580, Brazil

ARTICLE INFO

Keywords:
Xanthan gum
Amino acids
Coatings
Circular dichroism
Surface energy
Cell adhesion

ABSTRACT

In this work, citric acid molecules mediated simultaneously the crosslinking of xanthan gum (XG) chains and the grafting of glutamic acid (Glu), cysteine (Cys), histidine (His) or tryptophan (Trp) to XG chains, as evidenced by Fourier-transform infrared spectroscopy, elemental and thermogravimetric analyses, and high-resolution X-ray photoelectron spectroscopy. XG coatings (~60 nm thick) presented total surface energy (γS) of 65 mJ/m^2. The attachment of amino acids to the XG chains decreased γS values to ~ 48 mJ/m^2 because the surface energy polar (γ_pS) component decreased. Circular dichroism (CD) spectra revealed that the helix conformation of XG chains was retained in XG and XG-Glu-coatings, but it was lost in the XG-His, XG-Cys-and XG-Trp-coatings due to intermolecular interactions between the amino acid side groups (thiol, imidazole, and indole). XG-based coatings presented no cytotoxicity. After 3 h of incubation, the adhesion of SH-5YSY neural cells in comparison to the control (100%) was XG-His (18%), XG-Cys (21.4%), XG (29%), XG-Trp (28.6%) and XG-Glu (46.4%). The decrease of% cell adhesion tended to be favored by the decrease of γ_pS, except for XG-Glu-and XG-Trp, and by the loss of helix molecular conformation of chains in the coatings.

1. Introduction

Polysaccharides have been frequently applied in the development of biomedical devices due to their biocompatibility, water absorption, biodegradability, renewable sources, and the possibility to conjugate with others molecules (Bas, Catelas, De-Juan-Pardo & Hutmacher, 2018).

Cell adhesion might be undesirable for specific applications, such as for heart valves devices such as stents, implants, or even injection syringes because the cells are able to adhere and grow on the blood channel, blocking the blood flow (Khalili & Ahmad, 2015). Neural devices such as neural electrodes are a "hot topic" due to their capability of cell-stimulating and signal recording in the brain Yin, Liu, Xiao and Zhang (2021). However, the devices can fail due to fouling caused by astrocytes and microglial cells surrounding the electrode, promoting inflammation processes and scar formation (Polikov, Tresco & Reichert, 2005). This drawback can be overcome by the addition of anti-fouling coatings on the electrodes. For instance, in comparison to the uncoated neural silicon and iridium electrodes, microglia and astrocytes attached less after coating with poly(*N*-isopropyl acrylamide)-*co*-poly (acrylic acid) crosslinked with poly(ethylene glycol) (PEG) (Gutowski et al., 2014). Neural cell adhesion protein (L1) conjugated with PEG layer contributed to decreasing the astrocyte's attachment on silicon surfaces (Azemi, Stauffer, Gostock, Lagenaur & Cui, 2008). However, polysaccharide-based coatings designed for reducing cell adhesion are scarcely reported in the literature (F. Ceyssens et al., 2013; D.H. Kim, Wiler, Anderson, Kipke & Martin, 2010).

Xanthan gum (XG) produced by the bacteria genus *Xanthomonas* is a versatile polysaccharide, which has been applied in a wide range of technological fields (Petri, 2015). Fig. 1 represents the chemical structure of XG. The cellobiose repeating unit composes the backbone and the trisaccharide D-mannose (β−1,4) D-glucuronic acid (β−1,2) and D-mannose, which are attached to alternate glucose residues in the backbone by α−1,3 linkages, composes the side chain. D-mannose unit linked to the main chain contains an acetyl group at position *O*-6 and approximately one-half of the terminal D-mannose contains a pyruvic

* Corresponding author at: Instituto de Química, University of Sao Paulo, *Av* Prof Lineu Prestes 748, São Paulo, 05508000 Brazil.
E-mail addresses: dfsp@iq.usp.br, dfsp@usp.br (D.F.S. Petri).

https://doi.org/10.1016/j.carpta.2022.100227

Available online 11 June 2022

acid residue (Petri, 2015). At pH > 4, XG chains behave as polyanions due to the carboxylic acids deprotonation. XG has been applied for drug release (Bueno, Hilamatu, Carmona-Ribeiro & Petri, 2018), cartilage (Byram et al., 2020), probiotic co-encapsulation (Xiao et al., 2020), bowel healing (Huang et al., 2021), and scaffolds for neuronal differentiation (T. Glaser, Bueno, Cornejo, Petri & Ulrich, 2015; S. Kondaveeti, Semeano, Cornejo, Ulrich & Petri, 2018) due to its high biocompatibility. On the other hand, amino acids (AA) are interesting candidates for the decoration of thin films because they are fundamental organic molecules used for cell signaling, gene expression, proteins phosphorylation balance, and other biological molecules synthesis (e.g. basic unit to protein chain) (Wu, 2009). Glutamic acid (Glu) (Fig. 1), an anionic AA at pH 7.4, is responsible for immune function. Histidine (His) (Fig. 1), a cationic AA at pH 7.4, presents antioxidant and wound healing properties. Cysteine (Cys) (Fig. 1), a polar AA at pH 7.4, is an abundant source of sulfur (-SH thiol group), and tryptophan (Trp) (Fig. 1) is a hydrophobic AA with indole group.

In this work, XG coatings were individually crosslinked and decorated with Trp, His, Glu-and Cys-simultaneously on glass slides and Si wafers, with the aid of citric acid. Si wafers are generally used as substrates for neural electrodes and microelectronic devices. Citric acid (CA) is a low cost nontoxic crosslinker for polysaccharides (A.C. Alavarse et al., 2022; A.K. Antosik, Piątek & Wilpiszewska, 2019; M.A. Hussain, Kiran, Haseeb, Hussain & Hussain, 2020; Z. Qin, Jia, Liu, Kong & Wang, 2020; H. H. Wu et al., 2019). The hypothesis of this study is that the type of AA grafted to the XG coatings might affect the molecular conformation of XG chains confined in the coatings, coating surface energy and adhesion of cells on them.

2. Experimental

2.1. Materials

Xanthan gum (XG) (CP Kelco, Brazil) with degree of pyruvate of 0.39, degree of acetyl of 0.42, and M_v of 1.3×10^6 g/mol (**Supplementary Material SM1**) was used as received. L-cysteine (Cys), L-glutamic acid (Glu), L-histidine (His), L-tryptophan (Trp) amino acids were provided by Sigma Aldrich (Brazil); citric acid (CA) and sodium hypophosphite (SHP), hydrochloric acid (HCl) were purchased from Labsynth (Brazil). Silicon (100) wafers with native SiO_2 layer (University Wafer, USA) and glass coverslip (KASVI, Brazil) were cleaned with isopropanol prior to use.

2.2. Coating preparation

Solutions of 0.2 g/L XG, 0.2 g/L Cys, Glu, His-and Trp-were prepared separately in 0.01 mol/L HCl. The acid medium favors the crosslinking reaction and the solubility of AA. The crosslinking solution was composed by 1×10^{-2} g/L CA and 5×10^{-3} g/L SHP in a volume proportion to 4:1. XG, AA and crosslinking solutions were mixed in a volume proportion of 2:2:1 (XG:AA:CA/SHP) or 2:1 for XG:CA/SHP and homogenized for 0.5 h The precursor solutions covered the freshly rinsed Si wafers (~1 cm^2), which were kept overnight in an oven at 40 °C until complete evaporation of water. From this point on, ultrathin and thin coatings were prepared independently (Scheme 1). In order to obtain ultrathin films, a set of dry coatings was extensively rinsed in MilliQ, so that only XG chains and AA molecules closely bound to the silanol groups on the Si wafers or glass slides remained attached to the surface. Then, the samples were heated at 165 °C for 7 min in order to promote the crosslinking reaction and the grafting of AA to XG chains. Dry coatings or micrometric films prepared by casting were heated at 165 °C during 7 min. All coatings and micrometric films were rinsed in MilliQ water to remove reactants that were just physically bound. They were coded as XG (no addition of AA), XG-Cys, XG-Glu, XG-His-and XG-Trp.

2.3. Physicochemical characterization of XG based coatings and micrometric films

The mean thickness (d) values of ultrathin and thin coatings were determined by means of ellipsometry. Contact angle measurements were performed by the sessile drop method. The surface energy (γS) of the XG based thin coatings was assessed by means of contact angles (θ) performed with droplets (10 μL) of diiodomethane and water. The chemical composition on the thin coating surface was determined by X-ray photoelectron spectroscopy (XPS). Circular dichroism (CD)

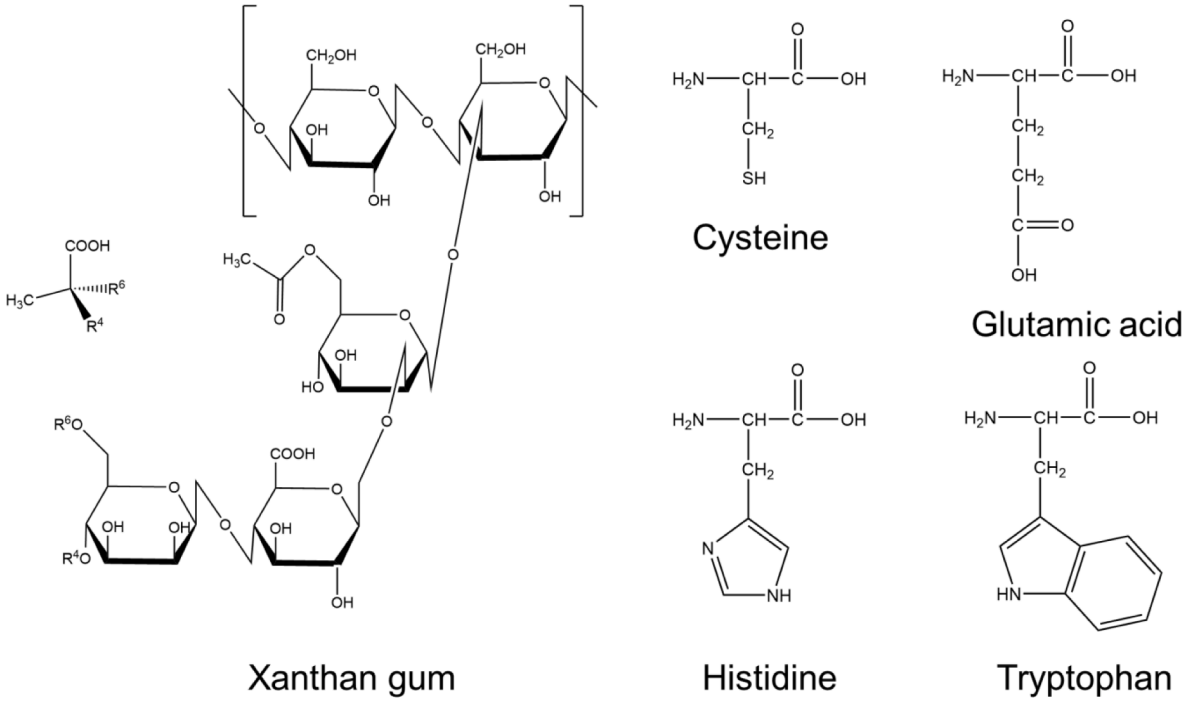

Fig. 1. Representation of chemical structures of xanthan repeated unit, cysteine (Cys), glutamic acid (Glu), histidine (His) and tryptophan (Trp).

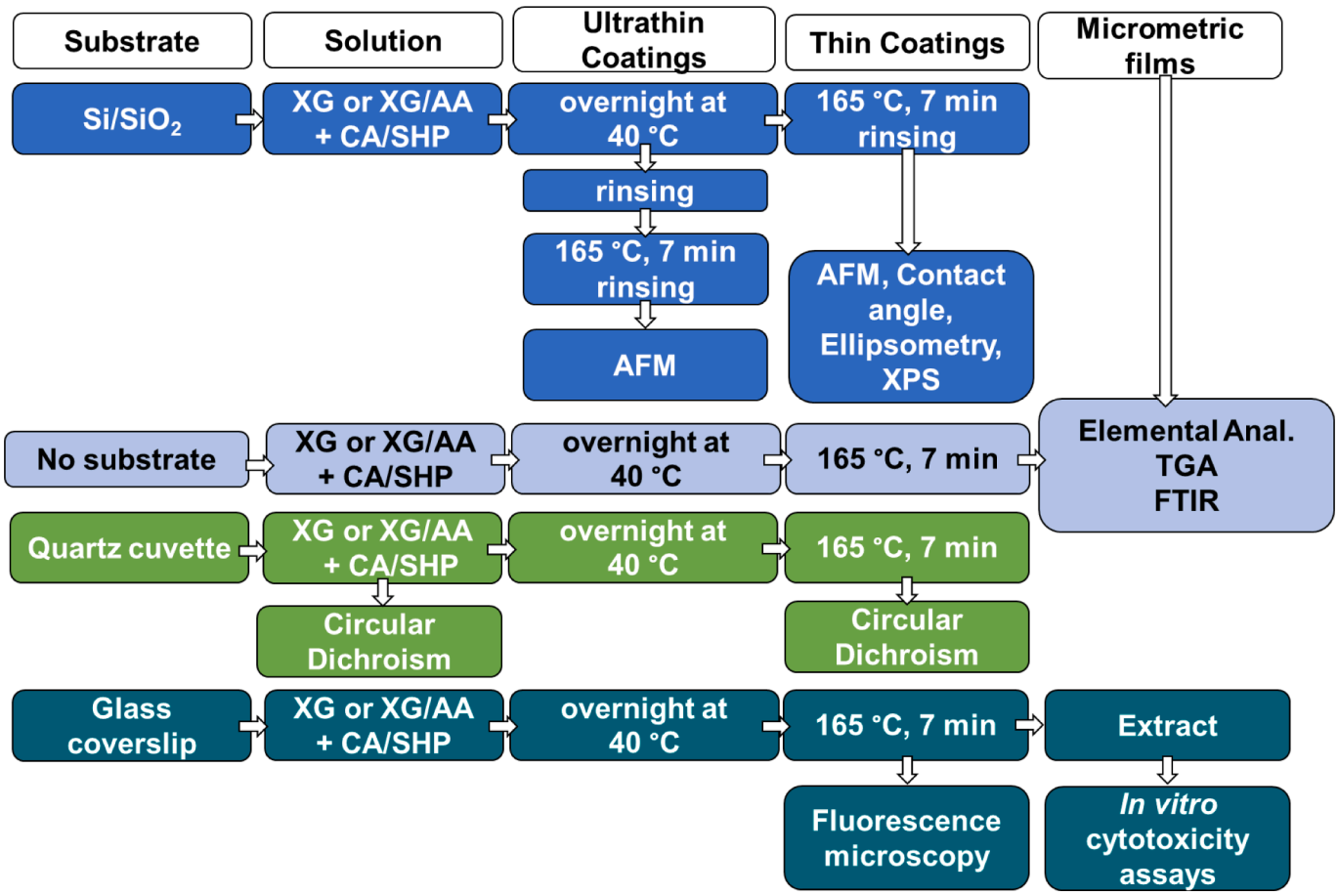

Scheme 1. Overview of experimental steps for the synthesis and characterization of XG-based coatings and films for the assays with cells.

measurements were performed on thin coatings deposited on the external wall of quartz cuvettes. Topography and surface roughness of ultrathin and thin films were analyzed by atomic force microscopy (AFM). XG (powder), Cys, Glu, His, Trp-and citric acid and XG, XG-Cys, XG-Glu, XG-His-and XG-Trp-micrometric (~ 50 μm thick) films were analyzed by Fourier-transform infrared vibrational spectroscopy in the attenuated total reflectance mode (FTIR-ATR). The amount of AA grafted to the XG chains was quantified by elemental analysis (CNH). The thermal behavior of XG, XG-Cys, XG-Glu, XG-His-and XG-Trp-micrometric (~ 50 μm thick) films and XG (powder) was investigated by thermogravimetric analyses (TGA). Details about equipment used and measurement conditions were provided as **Supplementary Material SM2**.

2.4. Cell adhesion and viability

SH-SY5Y neuroblastomas cells (ATCC, CRL-2266) cloned from human bone marrow tissue were used for the cell adhesion viability assays. The in vitro cytotoxicity assays were performed using the solution extract, according to H. ISO 10993–5:2009 (H. ISO 10993–5:2009 - Biological Evaluation of Medical Device), which involves the contact between cells seeded into the well plates with extract solution derived from the thin coatings. Metabolic activity was evaluated by the 3-(4, 5-dimethyl-2-thiazolyl)−2,5-diphenyl-2H-tetrazolium bromide (MTT) assay. The cell viability of each sample was tested in quintuplicate (n = 5), dividing the absorbance reading corresponding to the sample by the absorbance reading of the control. After running the MTT assays, the remaining solution from these tests was used to quantify the lactate dehydrogenase (LDH) activity with the aid of LDH Liquiform kit assay (Labtest, Brazil). In order to observe the cells' adhesion on the thin coatings, SH-SY5Y cells (5×10^5 cells/well) were cultivated for 3 h and 24 h After that, cells were fixed with paraformaldehyde solution (4%) for 30 min at 4 °C. The DNA of cell nuclei was stained with DAPI and the fluorescence microscopy images were recorded using an inverted fluorescence microscopy (Axiovert ZEISS, Germany) with an exposure time of 20 ms. The images were treated with ImageJ software (cell counter notice plug-in). The total cell count took into account the acquisition of three random images for each coating. Details about equipment used and measurement conditions were provided as **Supplementary Material SM3**.

3. Results and discussion

3.1. Crosslinking of xanthan gum chains and grafting of amino acids to them

The mechanism of crosslinking polysaccharides with polycarboxylic acids catalyzed by SHP involves the formation of anhydrides, and subsequent nucleophilic attack of polysaccharide hydroxyl groups to the anhydride, yielding ester linkages (A.C. Alavarse et al., 2022; V.S. Ghorpade, Dias, Mali & Mulla, 2019; B. Ji, Tang, Yan & Sun, 2015). Fig. 2**a** shows the FTIR spectra obtained for XG (powder), CA (powder) and XG crosslinked micrometric film. The spectra of XG powder and XG crosslinked film show the characteristic bands of polysaccharides in the 3500–3200 cm^{-1} region (OH vibrational stretching); at 2930 cm^{-1} and 2850 cm^{-1} (symmetrical and asymmetrical CH stretching); and in the 1240– 850 cm^{1} region (C–O and C–C stretching vibrations of the saccharide ring) (Silverstein, Bassler & Morrill, 1991). Particularly important are the intensities ratio between carbonyl stretch (C = O) bands at 1600 cm^{-1} and 1719 cm^{-1}, which correspond to the acidic and

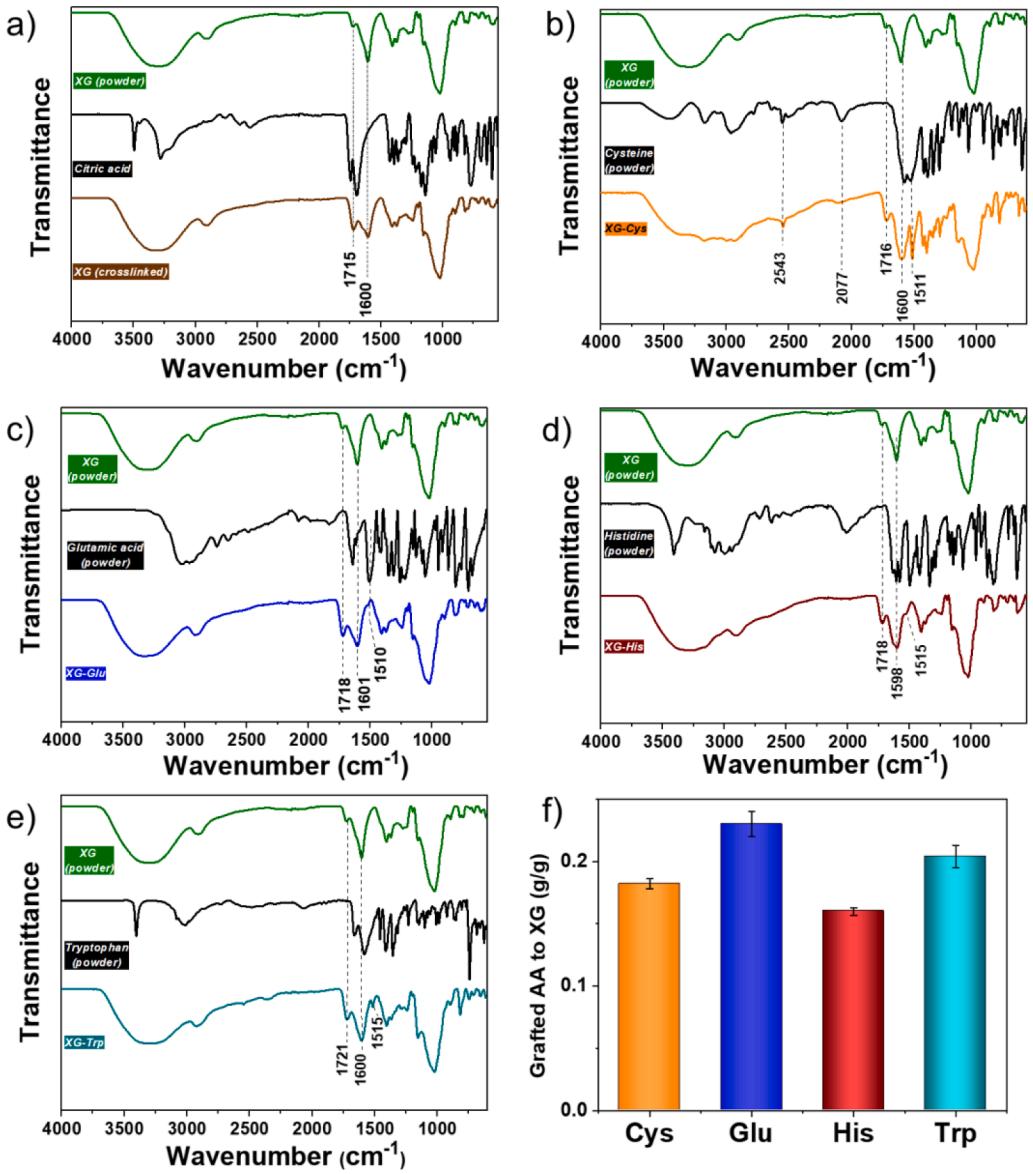

Fig. 2. FTIR-ATR spectra obtained for XG (powder), CA (powder), AA (powder), XG and XG-AA crosslinked micrometric films: (**a**) no AA, (b) AA = Cys, (c) AA = Glu, (**d**) AA = His-and (**e**) AA = Trp. (**f**) Amount of grafted AA (in gram) per gram of XG-AA film, calculated from CHN analyses (**Supplementary Material SM7**).

ester forms, respectively, I_{1600}/I_{1719}. For XG powder and XG films they amounted to 3.5 and 1.2 (**Supplementary Material SM4**), respectively, indicating the increase of ester linkages after crosslinking; a similar trend was observed in previous study about the crosslink of XG with citric acid (Bueno, Bentini, Catalani & Petri, 2013).

Figs. 2**b to** 2**e** show the FTIR-ATR spectra obtained for XG (powder), AA (powder) and XG-AA crosslinked micrometric films. In general, the spectra of XG-AA showed the characteristic bands of XG and the corresponding AA, as evidenced by the band assignments in the **Supplementary Material SM5**. The XG-Cys-spectrum (Fig. 2**b**) presented the carbonyl stretch (C = O) bands at 1600 cm^{-1} and 1716 cm^{-1} corresponding to the acidic and ester forms and typical bands of Cys-thiol and amine groups at 2543 cm^{-1} (S–H), 2077 cm^{-1} (stretching vibrations of $-NH_3^+$ group of L-cysteine) and 1511 cm^{-1} (bending N—H). The spectra of XG-Glu, XG-His-and XG-Trp-in Figs. 2**c,** 2**d** and 2**e**, respectively, presented the carbonyl stretch (C = O) bands at 1600 cm^{-1} and ~ 1718 cm^{-1} corresponding to the acidic and ester forms and at 1511 cm^{-1}, that was assigned to the bending N—H (Silverstein et al., 1991).

FTIR-ATR spectra provided qualitative evidences for the crosslinking and grafting of AA onto XG chains mediated by CA molecules. CA molecules attached to the XG chains can be converted to anhydride again, reacting with XG hydroxyl groups (crosslinking between XG chains, ester formation) or with AA amine groups (grafting of AA to the XG chains, amide formation) (Toledo, Bernardinelli, Sabadini & Petri, 2020), as depicted in the **Supplementary Material SM6**. In order to quantify the amount of AA grafted to the XG chains, elemental analyses (CHN) were performed for micrometric XG and XG-AA films (**Supplementary Material SM7**). Fig. 2**f** shows that in average the amount of grafted AA to the XG chains was ~ 0.20 g/g.

The effect of XG chains crosslinking and grafting of AA onto XG chains mediated by CA on their thermal stability was investigated by means of TGA (**Supplementary Material SM8**). All samples presented loss of water (8.9–15.5%) at temperatures lower than 100 °C. XG (powder) presented an event at 295 °C attributed to chain degradation (53.3% of mass loss); this event was also observed for XG and XG-AA films at similar temperature. After crosslinking XG chains with citric acid, a mass loss of 9.6% at 227 °C was attributed to the degradation of citric acid (Barbooti & Al-Sammerrai, 1986). XG-Cys, XG-Glu-and XG-His-also presented a mass loss at ~ 227 °C, whereas for XG-Trp-this event was at ~ 211 °C. The decomposition temperatures of pure Cys,

Glu-and His-are reported as 201 °C, 245 °C and 280 °C, respectively, with CO_2, NH_3 and H_2O as typical decomposition products (Weiss, Muth, Drumm & Kirchner, 2018). Under N_2 atmosphere pure Trp-presents two decomposition peaks, one at 304 °C and 415 °C, the latter results from the decomposition of the indole group (Da et al., 2015). XG-Cys, XG-Glu-and XG-His-films presented mass loss at ~ 200 °C that was attributed to the decomposition of amino acids. In the case of XG-Trp, the two decomposition peaks appeared at 272 °C and 362 °C. Except for Glu, grafting the AA to the XG chain decreased considerably their thermal stability.

3.2. Ultrathin XG based coatings

Fig. 3 shows AFM images (1 μm x 1 μm) of ultrathin (UT) coatings along with the corresponding roughness (rms) and mean thickness (d) values. The structures represent the arrangement of XG chains in the absence or presence of AA close to the Si/SiO_2 surface, which remained after extensively rinsing (Scheme 1). The isoelectric point of SiO_2 is reported as 2.8 (Chevalier et al., 2016). Thus at pH 2.0, most silanol groups tend to be positively charged and ion-dipole interactions with the XG and AA-Glu-chains are expected.

UT-XG (Fig. 3**a**) and UT-XG-Glu (Fig. 3**b**) were similar (d ~ 5–6 nm);

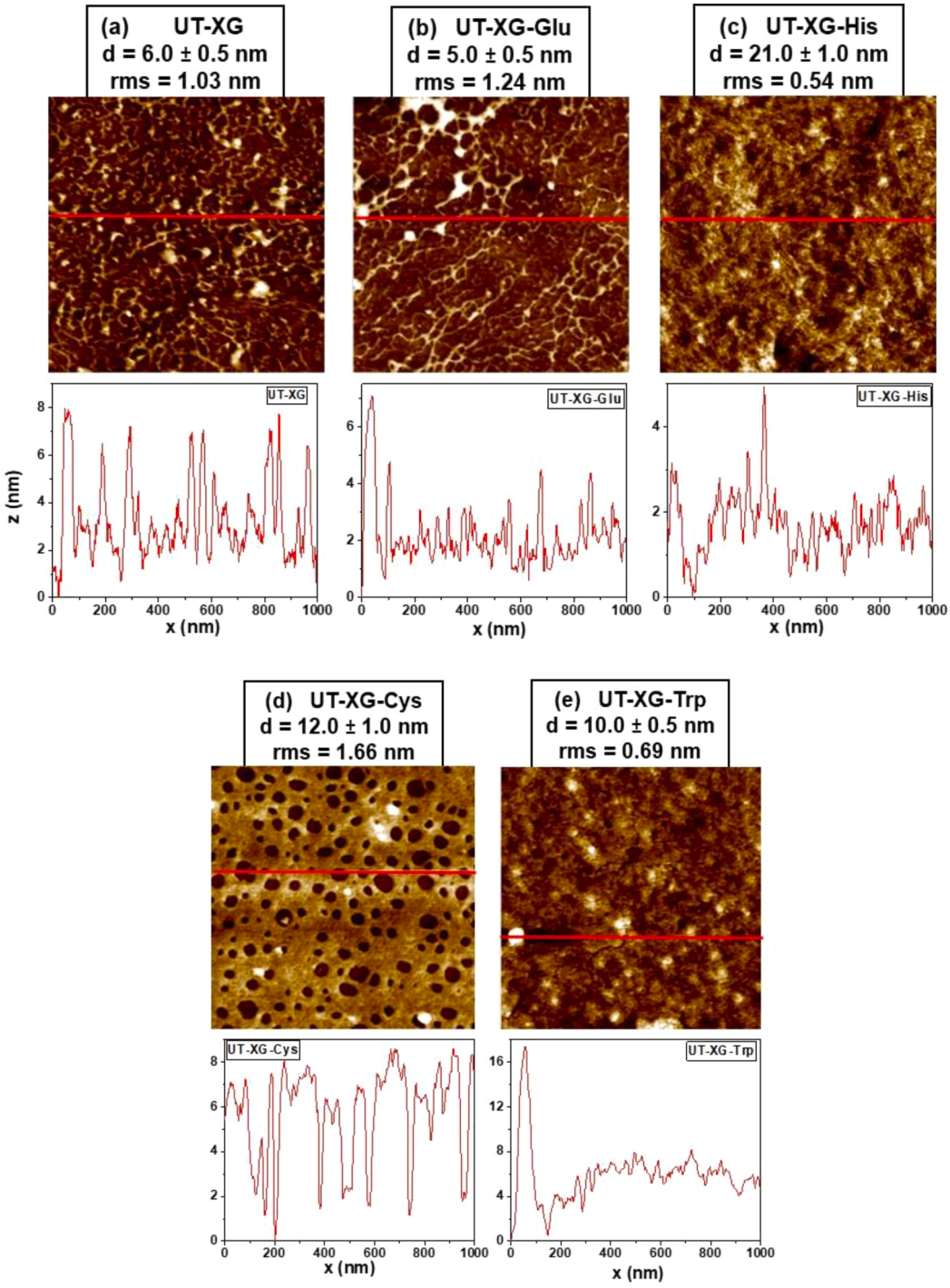

Fig. 3. AFM topographic images of ultra-thin coatings: UT-XG (**a**), UT-XG-Cys (**b**), UT-XG-Glu (**c**), UT-XG-His (**d**) and UT-XG-Trp (**e**). The red line represents the position corresponding to the cross-sections.

in both cases XG chains appear as crosslinked fibers and did not covered completely the underlying substrate. Similar fibrillar structures were observed by AFM for XG sample in air or liquid conditions (Liang et al., 2014) or in the presence of Ca^{2+} ions (Dário, Hortêncio, Sierakowski, Neto & Petri, 2011). The high molecular weight of XG chains and the transition from random coils conformation to ordered helix conformation driven by intermolecular interactions favor this kind of structural organization as fibers (Morris, Rees, Young, Walkinshaw & Darke, 1977) . At pH 2, the carboxylic acid groups belonging to XG and Glu-are protonated, favoring intermolecular H bonds.

The presence of a positively charged side chain in His-led to the formation of smooth and homogeneous UT-XG-His-coatings (Fig. 3**c**); the attachment of His-groups to XG chains might favor electrostatic interactions with neighbor chains and substrate, yielding thick (d ~ 20 nm) and uniform layers. The low polarity of thiol side group might have induced the formation of pores in UT-XG-Cys-coatings (Fig. 3**d**) during the drying process, resembling dewetting. On the other hand, the presence of hydrophobic indole group led to smooth UT-XG-Trp-coatings ~10 nm thick (Fig. 3**e**); the Trp-molecules grafted to the XG chains might interact with other by hydrophobic interactions among the indole groups, orientating to the air (hydrophobic medium). These findings indicated that the type of amino acid side group induced different interactions among the AA decorated XG chains and substrate, influencing the coating morphology.

3.3. Thin XG based coatings

The effect of AA type grafted to the XG chains on the morphology of thin ($d > 50$ nm) coatings was evaluated. Fig. 4 shows that networks of fibers or nanopores were not observed on thin coatings. Regardless of the AA type the surfaces presented similar features like rms and mean thickness values (Table 1). These findings indicate that the type of amino acid side group induced different interactions among the AA decorated XG chains only when the chains were confined as ultrathin films. Upon increasing the coating thickness, the influence of the intermolecular interactions became less pronounced and the chains arrangement was similar.

Table 1
Mean thickness (d) and roughness (rms) values determined for thin coatings ($n = 3$). Mean contact angle (θ) values determined for MilliQ water and CH_2I_2 droplets on XG based coatings, along with the polar (γ_pS) and dispersive (γ_dS) components of the surface energy (γS) ($n = 4$).

Sample	d (nm)	rms (nm)	θa (°) water	θa (°) CH_2I_2	γ_pS (mJ/m^2)	γ_dS (mJ/m^2)	γS (mJ/m^2)
XG	64.8 ± 5.6	12.0 ± 2.6	39 ± 4	40.2 ± 0.1	25 ± 2	40 ± 4	65 ± 6
XG-Cys	65 ± 15	15.7 ± 5.1	52 ± 5	39.5 ± 0.5	17 ± 2	40 ± 4	57 ± 6
XG-Glu	66.8 ± 9.5	23.0 ± 1.6	63 ± 6	46 ± 2	12 ± 1	37 ± 4	49 ± 5
XG-His	57 ± 14	23.6 ± 1.9	65 ± 5	47 ± 2	11 ± 1	36 ± 4	47 ± 5
XG-Trp	62 ± 12	12.0 ± 2.5	63 ± 5	47 ± 2	12 ± 1	36 ± 4	48 ± 5

Table 1 shows the contact angle (θ) values determined for MilliQ water and CH_2I_2 droplets on XG based coatings, along with the polar (γ_pS) and dispersive (γ_dS) components of the surface energy (γS). In comparison to pure XG, the attachment of amino acid to the XG chains did not affect the γ_dS component, but decreased considerably the γ_pS component. Thin films presented larger rms values (Table 1) than ultrathin films (Fig. 3), that probably caused deviations in the contact angle measurements of ~ 10%. The increase of surface roughness of Ti-6Al-4 V alloys caused variation in the γS values from 45 mJ/m^2 to 52 mJ/m^2 (Yan, Chibowski & Szcześ, 2017).

The chemical composition of thin coatings was analyzed by XPS. Fig. 5 shows the high-resolution XPS spectra for carbon (C 1 s), oxygen (O 1 s), nitrogen (N 1 s) and sulfur (S 2p) binding energy (BE) regions. The deconvolution of carbon satellite peak (C 1 s) for pure XG (no AA or

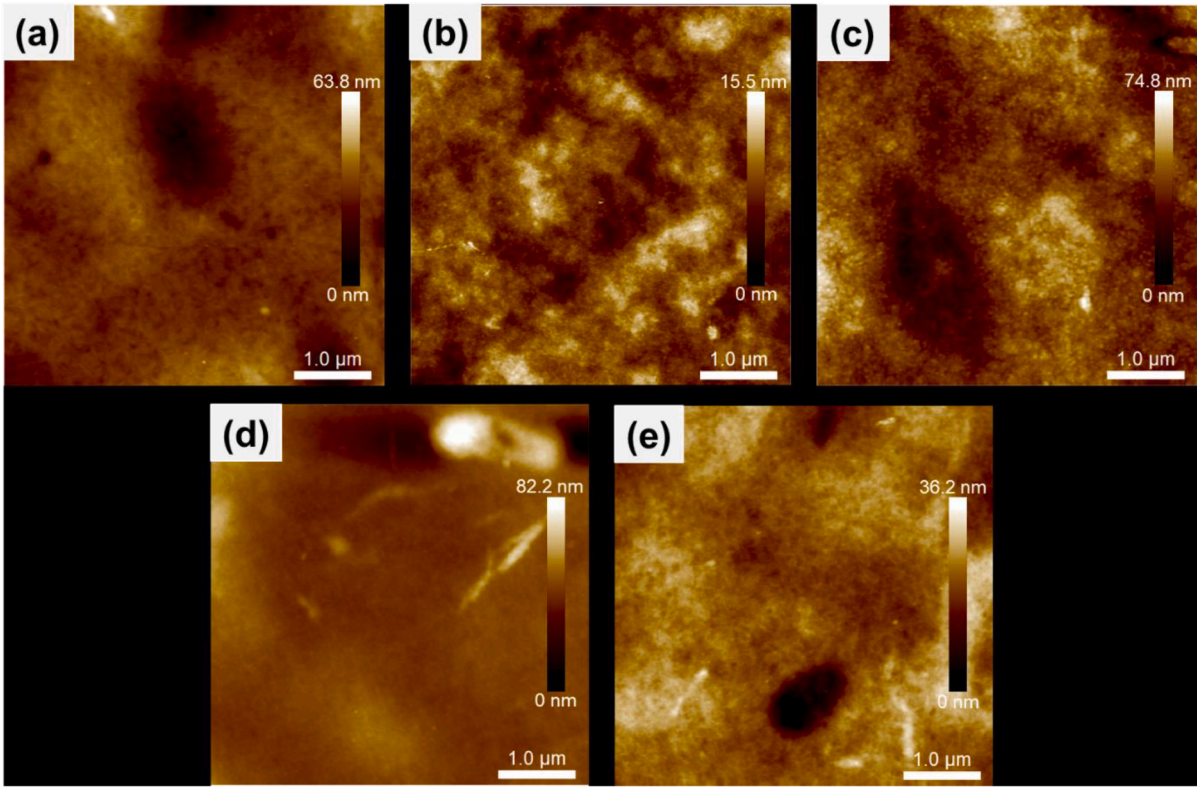

Fig. 4. AFM topographic images of (**a**) XG, (**b**) XG-Cys, (**c**) XG-Glu, (**d**) XG-His-and (**e**) XG-Trp-thin films.

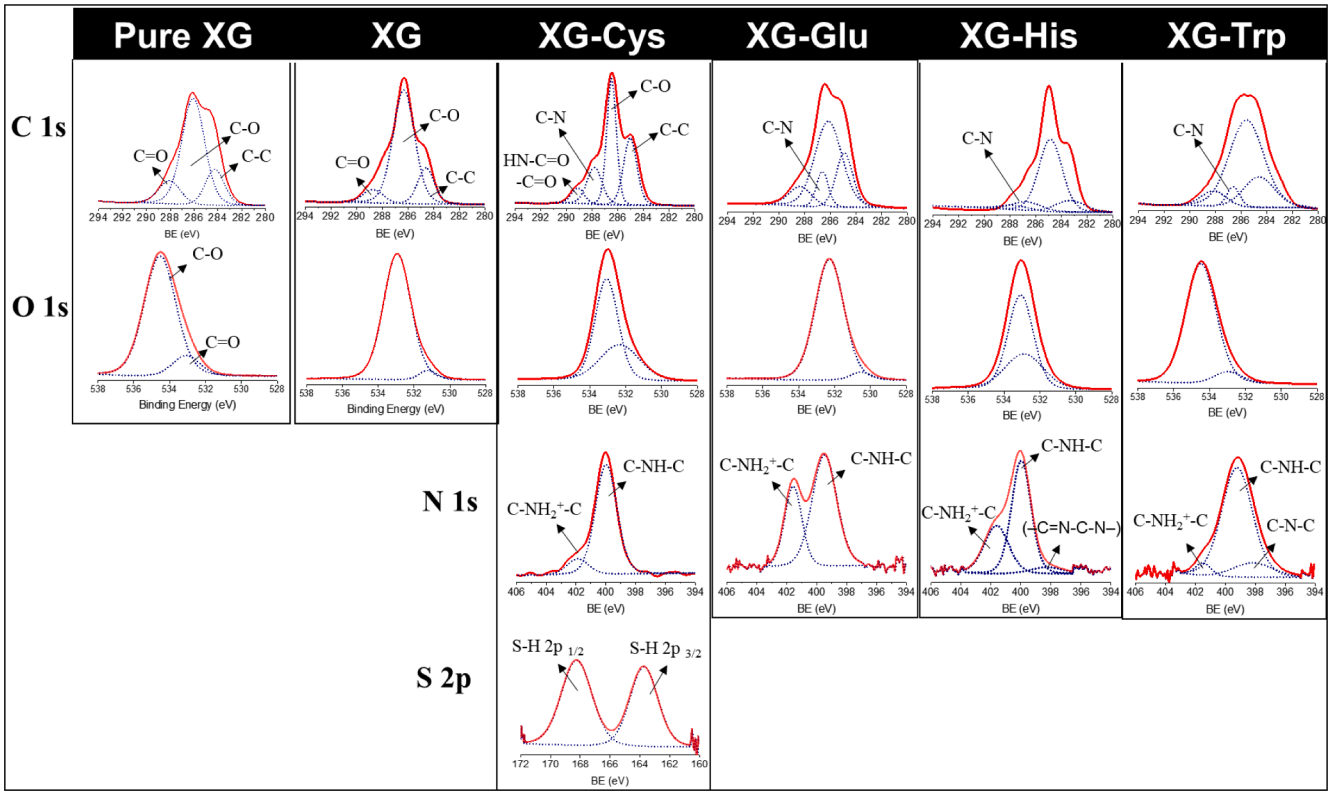

Fig. 5. Deconvolution of XPS high-resolution spectra of C 1 s, N 1 s, O 1 s and S 2p, along with the corresponding BE values determined for pure XG, XG coatings, XG-Cys, Glu, XG-His-and XG-Trp-coatings.

crosslinker) indicated three peaks attributed to C—C (284.5 eV) as dominant component, C—O (286.1 eV) and C = O (288.0 eV) bonds (Bulbul, Bhushette, Zambare, Deshmukh & Annapure, 2019). After crosslinking, XG coatings presented C 1 s peaks similar to those of pure XG; however, the intensity associated to C—O bond increased, confirming the esterification reaction between citric acid and XG hydroxyl groups. The grafting of amino acids to XG chains was identified by the appearance of a new peak in C 1 s region, typical of C—N bonds at 287.8 eV (XG-Cys), 286.3 eV (XG-Glu), 287.7 eV (XG-His), and 286.5 eV (XG-Trp) (A. Artemenko et al., 2021). Additionally, the acetamide (O =

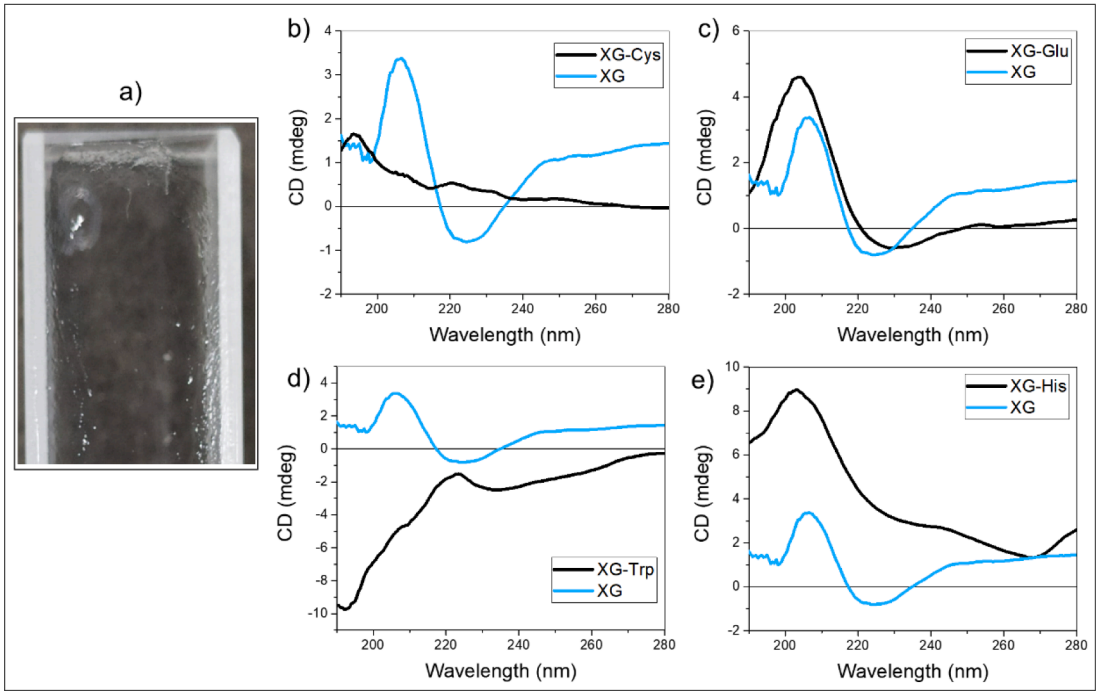

Fig. 6. (**a**) Photograph of a PBS swollen XG coating deposited on the cuvette for circular dichroism (CD) measurements. CD spectra of (**b**) XG (blue) and XG-Glu (black) coatings, (**c**) XG (blue) and XG-Cys (black) coatings, (**d**) XG (blue) and XG-His (black) coatings and (**e**) XG (blue) and XG-Trp (black) coatings.

C—N) bond appears mutually in the same BE region as C—N. In the case of N 1 s region, two peaks signals were assigned to secondary protonated amine (C—NH_2^+-C) and secondary amine (C—NH—C), due to the amide formation. A third peak for C = N at 398 eV was assigned to imidazole in XG-His-and indole in XG-Trp-coatings (A. Artemenko et al., 2021; O. Cavalleri et al., 2004; J.S. Stevens et al., 2013). XG-Cys-coatings presented doublet peaks at 164/168 eV BE related to $2p_{3/2}$ and $2p_{1/2}$ S-H bond, which is typical for Cys (J.S. Stevens et al., 2013). **Table SM3** comprises the peaks after deconvolution of XPS high-resolution spectra of C 1 s, N 1 s, O 1 s and S 2p, along with the corresponding BE values.

XPS analyses in Fig. 5 and **Supplementary Material SM9** supported the reactions mechanism evidenced by FTIR-ATR spectra (Fig. 2), where citric acid molecules mediated the crosslinking of XG chains and the grafting of amino acids. In order to investigate if these reactions affect the conformational state of XG chains, thin XG based coatings were analyzed by circular dichroism (CD). The coatings were kept swollen in PBS buffer (Fig. 6**a**) during the measurements. The CD spectra obtained for XG and XG-Glu-coatings **(**Fig. 6**b)** presented similar features. The positive signal at ~ 203 nm – 205 nm attributed to n → π* transition of the carboxylate groups of XG (D-glucuronic acid and pyruvate groups) (V.B. Bueno & Petri, 2014; N.M. Eren, Santos & Campanella, 2015), and the negative signal at ~ 220 nm due to XG acetate groups (V.B. Bueno & Petri, 2014) indicated the helix conformation of XG chains in XG and XG-Glu-coatings. Thus, the attachment of Glu-to the XG chains did not affect the helix conformation of XG chains in the swollen coatings. On the other hand, grafting Cys (Fig. 6**c**), His (Fig. 6**d**) and Trp (Fig. 6**e**) caused substantial changes in the conformational state of XG chains in the corresponding coatings. In the case of XG-Cys (Fig. 6**c**) and XG-His (Fig. 6**d**) coatings the positive signal in the range of 195 nm to 205 nm could be observed, but the negative signal disappeared, indicating that the helix conformation was partially lost. In the case of XG-Trp-coatings (Fig. 6**e**), the XG chains seem to have lost completely the ordered helix conformation, assuming random coil conformation. The changes in the molecular conformation of XG chains might be attributed to the interactions between the amino acid functional groups attached to the chains. Particularly in the case of XG-Trp-coatings, π-π interactions between Trp-indole groups can approximate XG chains segments, inducing conformational changes in the chains.

3.4. Cell adhesion and viability on thin XG based coatings

The cell adhesion and viability assays were performed on thin XG-based coatings because they are more uniform than the ultrathin films and coatings thicker than 50 nm proved to be more suitable for studies on cell behavior (Bhattacharyya, Xu, Deshmukh, Timmons & Nguyen, 2010). Fig. 7**a** shows the adhesion of SH-5YSY cells after 3 h and 24 h of incubation in comparison to the control (100%). After 3 h incubation, the lowest cell adhesion was observed for XG-His-and XG-Cys-coatings, 18% and 21.4%, respectively. XG and XG-Trp-coatings presented the intermediate adhesion rates, namely, 29% and 28.6%, respectively, and XG-Glu-coatings showed the highest adhesion (46.4%), in comparison to the control. Fig. 7**b** shows that the% cell adhesion tended to decrease with the decrease of γ_pS, except for XG-Glu-and XG-Trp. The adhesion of fibroblasts was very low on surfaces with low γ_pS values (polyolefin,

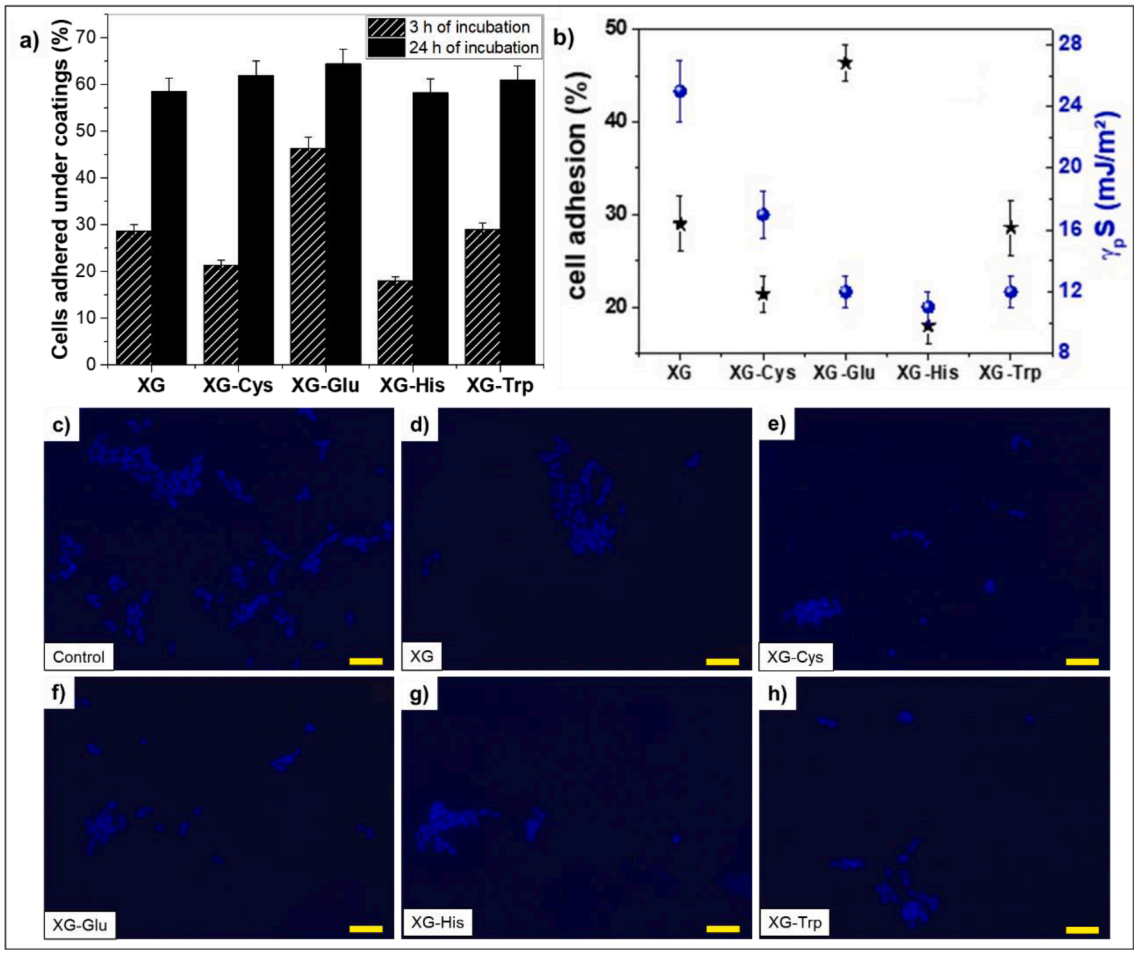

Fig. 7. (**a**) Cell adhesion (%) on XG-based coatings in comparison to the cell adhesion on the plastic cell plate after 3 h and 24 h incubation (error bars set to 5%).(**b**) Cell adhesion (%) after 3 h and the polar component of surface energy (γ_pS) determined for XG-based coatings. Fluorescence microscopy images (DAPI stained) of SH-S5YS cells incubated (24 h) on control (**c**), XG (**d**), XG-Cys (**e**), XG-Glu (**f**), XG-His) (**g**) and XG-Trp (**h**) coatings. Scale bar: 100 μm.

Teflon, silicone rubber), but increased considerably on more hydrophilic surfaces (glass, metals stainless steel, cobalt-chromium alloy, titanium alloy and tantalum) (Hallab, Bundy, O'Connor, Moses & Jacobs, 2004). Recently, Mahjy et al. prepared poly(dimethyl siloxane) with surface energy values ranging from 21 mJ/m^2 to 100 mJ/m^2 and roughness values ranging from 5 nm to 150 nm; surfaces with γS of ~ 70 mJ/m^2 and intermediate roughness values were the most favorable for the adhesion of cells (Majhy, Priyadarshini & Sen, 2021). Therefore, the low adhesion of cells on thin XG-based coatings can be attributed to the low roughness (~ 20 nm) and γS of ~50 mJ/m^2 (Table 1). The lowest cell adhesion on XG-His-and XG-Cys-coatings after 3 h incubation might also be correlated with the partial loss of helix conformation observed in Figs. 6**c** and 6**d**.

After 24 h incubation, all XG-based coatings presented similar cell adhesion of ~ 60% in comparison to the control (Fig. 7**a**). This finding indicated that the coating surface energy and chains molecular conformational state affected the cell adhesion mainly at short incubation time (3 h). As the incubation time increases, the surface roughness might increase due to the adhesion of the first cells. Moreover, for long incubation time (24 h), the coatings became swollen by the culture medium, minimizing the effects of the surface energy components observed in the short incubation time. A similar trend was observed for the adhesion of MG-63 cells on poly(methyl methacrylate) (PMMA), polystyrene (PS), and poly(dimethyl siloxane) (PDMS) at 1 and 3 h incubation (Comelles, Estévez, Martínez & Samitier, 2010). Figs. 7**c**-7**h** show the fluorescence images of SH-SY5Y cells stained with DAPI on XG based coatings along with the control experiment after 24 h incubation. They clearly showed less pronounced cell adhesion on the XG coatings in comparison to the adhesion on the control.

In vitro biocompatibility of XG-based coatings was evaluated by MTT test with the extract solution resulting from the coating in contact with cell culture medium (24 h). After 24 h of cell incubation, none of the XG

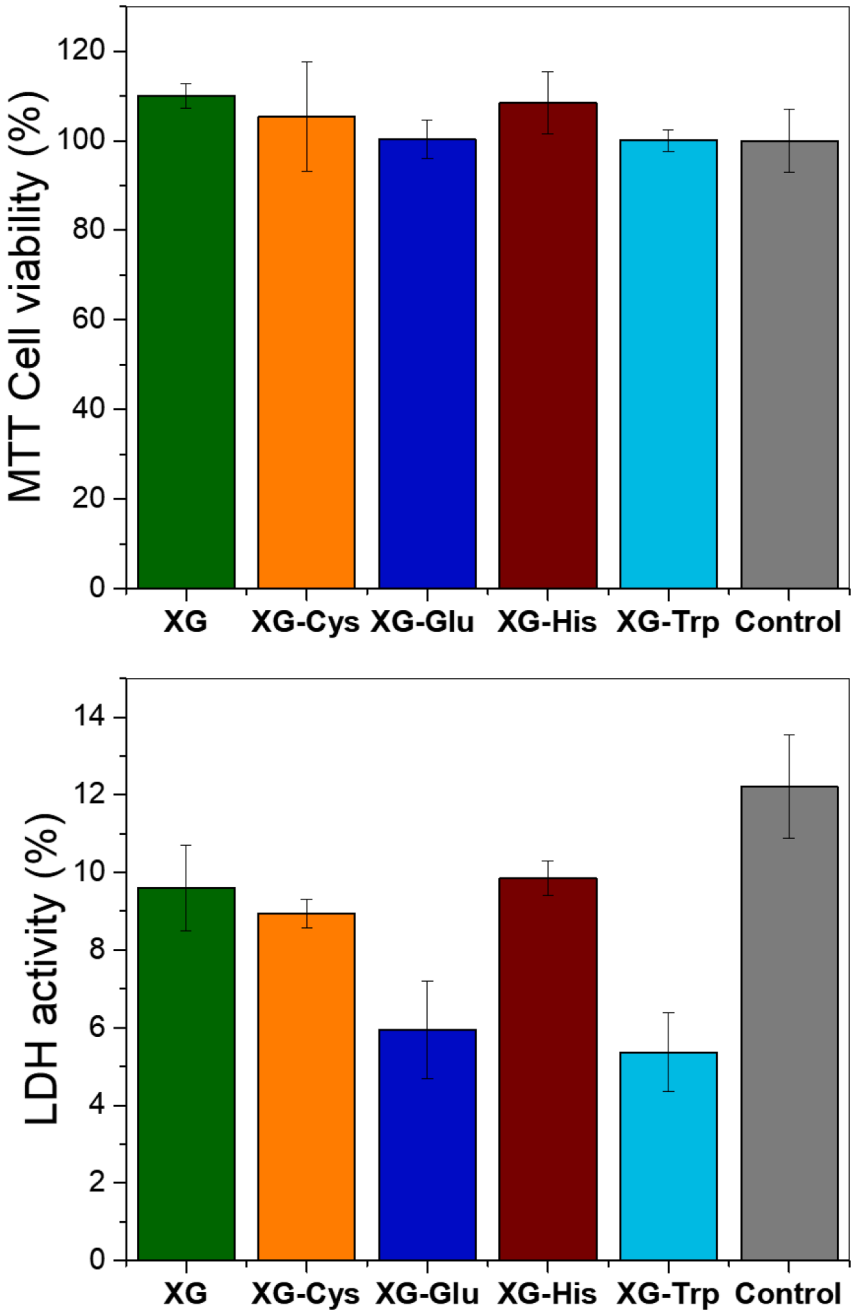

Fig. 8. (**a**) Cell viability (SH-SY5Y) of XG-based coatings using MTT assay and (**b**) Lactose dehydrogenase activity tests in the culture medium incubated for 24 h.

based coatings showed cytotoxicity (Fig. 8**a**). The amount of dead cells on the extract solutions was evaluated by the LDH assay (Fig. 8**b**). XG, XG-Cys-and XG-His-coatings showed LDH activity similar to the control; whereas the LDH values for XG-Glu-and XG-Trp-coatings were the lowest.

4. Conclusions

The crosslinking of XG chains and the grafting of AA onto XG chains mediated by CA molecules were clearly evidenced by FTIR-ATR spectra and TGA. Elemental analyses indicated ~ 0.20 g/g of AA grafted to XG chains. Thin (~ 60 nm) XG-amino acid coatings were successfully deposited on Si/SiO_2 wafers, quartz cuvettes and glass slides. In comparison to pure XG coatings, the grafting of Glu, Cys, His-or Trp-to the XG chains did not affect the dispersive surface energy (γ_dS) component, but decreased considerably the polar surface energy (γ_pS) component, making the adhesion of SH-SY5Y cells on them less than 30% or 60% of that observed for the control (plastic plate) after 3 h or 24 h incubation, respectively. The lowest cell adhesion after 3 h incubation observed for Cys-or His-grafted to XG coatings might also have been caused by the less ordered conformational state of chains observed in the CD spectra. The intermolecular interactions between Cys, His-and Trp-functional side groups affected the conformational state of XG chains in the corresponding coatings. Considering that none of the XG-amino acid coatings presented cytotoxicity against SH-SY5Y cells, all of them are potential candidates as coatings for neural electrodes. Nevertheless, for short incubation time, the XG-His (lowest γ_pS and random molecular conformational) is the most adequate to hinder cell adhesion on the coating.

Declaration of Competing Interest

The authors declare that they have no known competing financial interests or personal relationships that could have appeared to influence the work reported in this paper.

Acknowledgements

A.C.A. gratefully acknowledges São Paulo Research Foundation (FAPESP 2020/ 01907–3) for financial support. D.F.S.P. gratefully acknowledges financial support from CNPq (Grant 304017/2021–3) and FAPESP (Grant 2018/13492–2). E.C.G.F. gratefully acknowledges financial support from the Coordenação de Aperfeiçoamento de Pessoal de Nível Superior - Brasil (CAPES) - Finance Code 001 (Grant 88882.328247/2019–01). H.U. is grateful for grant support from FAPESP (2018/07366–4). The authors thank NAP-Phototech for the fluorescence microscopy facility.

Supplementary materials

Supplementary material associated with this article can be found, in the online version, at doi:10.1016/j.carpta.2022.100227.

References

Alavarse, A. C., Frachini, E. C. G., da Silva, R. L. C. G., Lima, V. H., Shavandi, A., & Petri, D. F. S. (2022). Crosslinkers for polysaccharides and proteins: Synthesis conditions, mechanisms, and crosslinking efficiency, a review. *International Journal of Biological Macromolecules, 202*, 558–596.

Antosik, A. K., Piątek, A., & Wilpiszewska, K. (2019). Carboxymethylated starch and cellulose derivatives-based film as human skin equivalent for adhesive properties testing. *Carbohydrate Polymers, 222*, Article 115014.

Artemenko, A., Shchukarev, A., Štenclová, P., Wågberg, T., Segervald, J., Jia, X., et al. (2021). Reference XPS spectra of amino acids. *IOP Conference Series: Materials Science and Engineering, 1050*(1), Article 012001.

Azemi, E., Stauffer, W. R., Gostock, M. S., Lagenaur, C. F., & Cui, X. T. (2008). Surface immobilization of neural adhesion molecule L1 for improving the biocompatibility of chronic neural probes: In vitro characterization. *Acta Biomaterialia, 4*(5), 1208–1217.

Barbooti, M. M., & Al-Sammerrai, D. A. (1986). Thermal decomposition of citric acid. *Thermochimica Acta, 98*, 119–126. C.

Bas, O., Catelas, I., De-Juan-Pardo, E. M., & Hutmacher, D. W. (2018). The quest for mechanically and biologically functional soft biomaterials via soft network composites. *Advanced Drug Delivery Reviews, 132*, 214–234.

Bhattacharyya, D., Xu, H., Deshmukh, R. R., Timmons, R. B., & Nguyen, K. T. (2010). Surface chemistry and polymer film thickness effects on endothelial cell adhesion and proliferation. *Journal of Biomedical Materials Research Part A, 94A*(2), 640–648.

Bueno, P. V. A., Hilamatu, K. C. P., Carmona-Ribeiro, A. M., & Petri, D. F. S. (2018). Magnetically triggered release of amoxicillin from xanthan/Fe3O4/albumin patches. *International Journal of Biological Macromolecules, 115*, 792–800.

Bueno, V. B., Bentini, R., Catalani, L. H., & Petri, D. F. S. (2013). Synthesis and swelling behavior of xanthan-based hydrogels. *Carbohydrate Polymers, 92*(2), 1091–1099.

Bueno, V. B., & Petri, D. F. S. (2014). Xanthan hydrogel films: Molecular conformation, charge density and protein carriers. *Carbohydrate Polymers, 101*, 897–904.

Bulbul, V. J., Bhushette, P. R., Zambare, R. S., Deshmukh, R. R., & Annapure, U. S. (2019). Effect of cold plasma treatment on Xanthan gum properties. *Polymer Testing, 79*, Article 106056.

Byram, P. K., Sunka, K. C., Barik, A., Kaushal, M., Dhara, S., & Chakravorty, N. (2020). Biomimetic silk fibroin and xanthan gum blended hydrogels for connective tissue regeneration. *International Journal of Biological Macromolecules, 165*(A), 874–882.

Cavalleri, O., Gonella, G., Terreni, S., Vignolo, M., Floreano, L., Morgante, A., , … Rolandi, R., et al. (2004). High resolution X-ray photoelectron spectroscopy of L-cysteine self-assembled films. *Physical Chemistry Chemical Physics, 6*(15), 4042–4046.

Ceyssens, F., Van Kuyck, K., Vande Velde, G., Welkenhuysen, M., Stappers, L., Nuttin, B., Puers, R., et al. (2013). Resorbable scaffold based chronic neural electrode arrays. *Biomedical Microdevices, 15*(3), 481–493.

Cloarec, J. P., Chevalier, C., Genest, J., Beauvais, J., Chamas, H., Chevolot, Y., Baron, T., Souifi, A., et al. (2016). pH driven addressing of silicon nanowires onto Si3N4/SiO2 micro-patterned surfaces. *Nanotechnology, 27*(29), Article 295602.

Comelles, J., Estévez, M., Martínez, E., & Samitier, J. (2010). The role of surface energy of technical polymers in serum protein adsorption and MG-63 cells adhesion. *Nanomedicine: Nanotechnology, Biology and Medicine, 6*(1), 44–51.

Da, S., Mello, G., De, P., Cardoso, A., Oliveira, E. W. R. S., & Siqueira, A. B. (2015). Tryptophan. *Journal of Thermal Analysis and Calorimetry, 3*(122), 1395–1401.

Dário, A. F., Hortêncio, L. M. A., Sierakowski, M. R., Neto, J. C. Q., & Petri, D. F. S. (2011). The effect of calcium salts on the viscosity and adsorption behavior of xanthan. *Carbohydrate Polymers, 84*(1), 669–676.

Eren, N. M., Santos, P. H. S., & Campanella, O. (2015). Mechanically modified xanthan gum: Rheology and polydispersity aspects. *Carbohydrate Polymers, 134*, 475–484.

Ghorpade, V. S., Dias, R. J., Mali, K. K., & Mulla, S. I. (2019). Citric acid crosslinked carboxymethylcellulose-polyvinyl alcohol hydrogel films for extended release of water soluble basic drugs. *Journal of Drug Delivery Science and Technology, 52*, 421–430.

Glaser, T., Bueno, V. B., Cornejo, D. R., Petri, D. F. S., & Ulrich, H. (2015). Neuronal adhesion, proliferation and differentiation of embryonic stem cells on hybrid scaffolds made of xanthan and magnetite nanoparticles. *Biomedical Materials, 10*, Article 045002.

Gutowski, S. M., Templeman, K. L., South, A. B., Gaulding, J. C., Shoemaker, J. T., & LaPlaca, M. C. (2014). Host response to microgel coatings on neural electrodes implanted in the brain. *Journal of Biomedical Materials Research Part A, 102*(5), 1486–1499.

Hallab, N. J., Bundy, K. J., O'Connor, K., Moses, R. L., & Jacobs, J. J. (2004). Evaluation of metallic and polymeric biomaterial surface energy and surface roughness characteristics for directed cell adhesion. *Tissue Engineering Part A, 7*(1), 55–70.

Huang, J., Jiang, Y., Liu, Y., Ren, Y., Xu, Z., Li, Z., , … Ren, J., et al. (2021). Marine-inspired molecular mimicry generates a drug-free, but immunogenic hydrogel adhesive protecting surgical anastomosis. *Bioactive Materials, 6*(3), 770–782.

Hussain, M. A., Kiran, L., Haseeb, M. T., Hussain, I., & Hussain, S. Z. (2020). Citric acid crosslinking of mucilage from Cydonia oblonga engenders a superabsorbent, pH-sensitive and biocompatible polysaccharide offering on-off swelling and zero-order drug release. *Journal of Polymer Research, 27*, 49.

ISO - ISO 10993-5:(2009). - Biological evaluation of medical devices — Part 5: Tests for in vitro cytotoxicity. (n.d.). Retrieved May 22, 2022, from https://www.iso.org/standard/36406.html.

Ji, B., Tang, P., Yan, K., & Sun, G. (2015). Catalytic actions of alkaline salts in reactions between 1,2,3,4-butanetetracarboxylic acid and cellulose: II. Esterification. *Carbohydrate Polymers, 132*, 228–236.

Khalili, A. A., & Ahmad, M. R. (2015). A review of cell adhesion studies for biomedical and biological applications. *International Journal of Molecular Sciences, 16*(8), 18149–18184.

Kim, D. H., Wiler, J. A., Anderson, D. J., Kipke, D. R., & Martin, D. C. (2010). Conducting polymers on hydrogel-coated neural electrode provide sensitive neural recordings in auditory cortex. *Acta Biomaterialia, 6*(1), 57–62.

Kondaveeti, S., Semeano, A. T. S., Cornejo, D. R., Ulrich, H., & Petri, D. F. S. (2018). Magnetic hydrogels for levodopa release and cell stimulation triggered by external magnetic field. *Colloids and Surfaces B: Biointerfaces, 167*, 415–424.

Liang, H., Zeng, G., Li, Y., Zhang, S., Zhao, H., Guo, L., , … Dong, M., et al. (2014). Exploring the complex mechanical properties of xanthan scaffolds by AFM-based force spectroscopy. *Beilstein Journal of Nanotechnology, 5*, 365–373.

Majhy, B., Priyadarshini, P., & Sen, A. K. (2021). Effect of surface energy and roughness on cell adhesion and growth – facile surface modification for enhanced cell culture. *RSC Advances, 11*(25), 15467–15476.

Morris, E. R., Rees, D. A., Young, G., Walkinshaw, M. D., & Darke, A. (1977). Order-disorder transition for a bacterial polysaccharide in solution. A role for

polysaccharide conformation in recognition between Xanthomonas pathogen and its plant host. *Journal of Molecular Biology, 110*(1), 1–16.
Petri, D. F. S. (2015). Xanthan gum: A versatile biopolymer for biomedical and technological applications. *Journal of Applied Polymer Science, 132*(23), 42035.
Polikov, V. S., Tresco, P. A., & Reichert, W. M. (2005). Response of brain tissue to chronically implanted neural electrodes. *Journal of Neuroscience Methods, 148*(1), 1–18.
Qin, Z., Jia, X., Liu, Q., Kong, B., & Wang, H. (2020). Enhancing physical properties of chitosan/pullulan electrospinning nanofibers via green crosslinking strategies. *Carbohydrate Polymers, 247*, Article 116734.
Silverstein, R. M., Bassler, G. C., & Morrill, T. (1991). Spectrometric Identification of Organic Compounds. (5th ed.). New York: Wiley, (Chapter 3).
Stevens, J. S., de Luca, A. C., Pelendritis, M., Terenghi, G., Downes, S., & Schroeder, S. L. M. (2013). Quantitative analysis of complex amino acids and RGD peptides by X-ray photoelectron spectroscopy (XPS). *Surface and Interface Analysis, 45*(8), 1238–1246.
Toledo, P. V. O., Bernardinelli, O. D., Sabadini, E., & Petri, D. F. S. (2020). The states of water in tryptophan grafted hydroxypropyl methylcellulose hydrogels and their effect on the adsorption of methylene blue and rhodamine B. *Carbohydrate Polymers, 248*, Article 116765.
Weiss, I. M., Muth, C., Drumm, R., & Kirchner, H. O. K. (2018). Thermal decomposition of the amino acids glycine, cysteine, aspartic acid, asparagine, glutamic acid, glutamine, arginine and histidine. *BMC Biophysics, 11*(1), 1–15.
Wu, G. (2009). Amino acids: Metabolism, functions, and nutrition. *Amino acids, 37*(1), 1–17.
Wu, H., Lei, Y., Lu, J., Zhu, R., Xiao, D., Jiao, C., , … Li, M., et al. (2019). Effect of citric acid induced crosslinking on the structure and properties of potato starch/chitosan composite films. *Food Hydrocolloids, 97*, Article 105208.
Xiao, Y., Han, C., Yang, H., Liu, M., Meng, X., & Liu, B. (2020). Layer (whey protein isolate) -by-layer (xanthan gum) microencapsulation enhances survivability of L. bulgaricus and L. paracasei under simulated gastrointestinal juice and thermal conditions. *International Journal of Biological Macromolecules, 148*, 238–247.
Yan, Y., Chibowski, E., & Szcześ, A. (2017). Surface properties of Ti-6Al-4V alloy part I: Surface roughness and apparent surface free energy. *Materials Science and Engineering: C, 70*, 207–215.
Yin, P., Liu, Y., Xiao, L., & Zhang, C. (2021). Advanced metallic and polymeric coatings for neural interfacing: structures, properties and tissue responses. *Polymers, 13*, 2834.